Published in final edited form as:
Bioconjug Chem. 2008 January ; 19(1): 225–234. doi:10.1021/bc7003022.

A Novel Near-Infrared Fluorescent Integrin Targeted DFO Analog

Yunpeng Ye, **Sharon Bloch**, **Baogang Xu**, and **Samuel Achilefu**†
Department of Radiology, Washington University, St. Louis, MO 63110

Abstract

Desferrioxamine (DFO), a siderophore initially isolated from *Streptomyces pilosus*, possesses extraordinary metal binding properties with wide biomedical applications that include chelation therapy, nuclear imaging, and anti-proliferation. In this work, we prepared a novel multifunctional agent consisting of (i) a near-infrared (NIR) fluorescent probe–cypate; (ii) an integrin $\alpha_v\beta_3$ receptor (ABIR)-avid cyclic RGD peptide, and (iii) a DFO moiety, DFO-cypate-cyclo[RGDfK(~)] (**1**, ~ representing cypate conjugation site at the side chain of lysine; f is D-phenylalanine). Compound **1** and two control compounds, cypate-cyclo[RGDfK(~)] (**2**) and cypate-DFO (**3**), were synthesized by modular assembly of the corresponding protected RGD peptide cyclo[R(Pbf)GD(OBut)fK] and DFO on the dicarboxylic acid-containing cypate scaffold in solution. The three compounds exhibited similar UV-Vis and emission spectral properties. Metal binding analysis shows that DFO as well as **1** and **3** exhibited relatively high binding affinity with Fe(III), Al(III), and Ga(III). In contrast to Ga (III), the binding of Feto **1** and **3** quenched the fluorescence emission of cypate significantly, suggesting an efficient metal-mediated approach to perturb the spectral properties of NIR fluorescent carbocyanine probes. In vitro, **1** showed a high ABIR binding affinity (10^{-7} M) comparable to **2** and the reference peptide cyclo(RGDfV), indicating that both DFO and cypate motifs did not interfere significantly with the molecular recognition of the cyclic RGD motif with ABIR. Fluorescence microscopy showed that internalization of **1** and **2** in ABIR-positive A549 cells at 1 h post-incubation was higher than **3** and cypate alone, demonstrating that incorporating ABIR-targeting RGD motif could improve cellular internalization of DFO analogs. The ensemble of these findings demonstrate the use of multifunctional NIR fluorescent ABIR-targeting DFO analogs to modulate the spectral properties of the NIR fluorescent probe by the chelating properties of DFO and visualize intracellular delivery of DFO by receptor-specific peptides. These features provide a strategy to explore the potential of **1** in tumor imaging, and treatment as well as some molecular recognition processes mediated by metal ions.

INTRODUCTION

Recent research efforts have demonstrated that molecular imaging is a powerful tool for localizing, identifying, and characterizing a host of disease-specific targets. Examples include imaging molecular interactions, cell trafficking, tumor vitality, cell proliferation, apoptosis, angiogenesis, and response to treatment. In particular, optical molecular imaging holds great promise to accelerate drug discovery and development, including compound screening, lead discovery, optimization, pharmacokinetic studies, and clinical trials (1–3).

An attractive feature of optical imaging is its ability to unravel the molecular basis of cancers and other diseases, thereby providing vital information for diagnosing, staging, and monitoring therapeutic response (4–6). These applications emanate from numerous advantages of optical methods, including high detection sensitivity, real-time monitoring, convenience, and accessibility. In contrast to other established imaging methods such as radionuclear and x-ray

†corresponding author 4525 Scott Avenue, St. Louis, MO 63110, Phone: 314-362-8599, Fax: 314-747-5191, achilefus@mir.wustl.edu.

computed tomography, the use of low energy (non-ionizing) radiation for optical imaging provides additional benefit, especially in longitudinal studies. Over the past years, tremendous progress has been made in the development of optical contrast agents for in vivo tumor optical imaging. For instance, we and others have focused developed NIR fluorescent probes such as cyanine dyes and their bioconjugates, including somatostatin and RGD peptide analogs, as optical contrast agents for in vitro and in vivo tumor optical imaging (7–13). These results have inspired us to further apply optical imaging and related optical contrast agents in the discovery and development of novel, multifunctional, and targeted oncologic drugs. For example, the biological properties of therapeutic agents such as desferrioxamine (DFO) can be altered by linkage to a target-specific NIR fluorescent probe and the intracellular transport visualized by optical methods.

DFO, a siderophore initially isolated from *Streptomyces pilosus*, is a selective iron chelator (14). This siderphore and some analogs have been used in chelation therapy to treat iron-overload diseases such as thalassemia, sickle-cell anemia and hemochromatosis (15–17). DFO has also been shown to possess antiproliferative activities and clinical studies have demonstrated its potential as an adjunct to chemotherapy regimens (18–21). Its radiosensitizing activities have been utilized in radiation oncology(22). DFO has also served as a good chelator for radioactive metals in cancer nuclear imaging as demonstrated by the use of radioactive ^{67}Ga/^{68}Ga-[DFO]-octreotide to image somatostatin receptor-positive tumors by positron emission tomography of (23). Despite its lack of oral bioavailability and difficulties in patient compliance, the continued use of DFO in clinical settings strongly attests to its great potential in biomedical applications. It further suggests the potential use of DFO as a lead compound for discovering and developing novel DFO analogs and synthetic mimetics with improved biological properties and activities (24–27). However, the biological activity of DFO is not targeted to a specific molecular process and its hydrophilic nature limits its internalization in cells. For these reasons, conjugation of DFO with a receptor-specific ligand such as $\alpha_v\beta_3$ integrin receptor (ABIR)-avid RGD peptide could overcome these problems.

Integrins are heterodimeric cell surface receptors that mediate cell-cell and cell-matrix adhesion, metastasis, and angiogenesis processes (28–31). In particular, the over-expression of ABIR on activated endothelial cells in the neovasculature of tumors such as breast cancer, lung carcinomas, melanomas, and glioblastomas has been correlated with tumor growth, invasion and metastasis. Therefore, ABIR is an attractive molecular target for tumor imaging, early diagnosis, and therapy (32–37). Diverse ligands, including peptides and peptidomimetics have been found to interact with ABIR. Some of the high ABIR binding peptides have been successfully used to elucidate the structure and mechanisms as well as targeted delivery of NIR fluorescent probes, radionuclides, and anticancer agents (38–44).

In this study, we report the synthesis and in vitro evaluation of **1** and its two analogs i.e. Cypate-[RGDfK(~)] (**2**) and cypate-DFO (**3**) for targeting ABIR (Figure 1). The RGD peptide in the novel multifunctional NIR fluorescent RGD-bearing DFO (**1**) enhanced cellular uptake of DFO. We also found that metal chelating properties of DFO can modulate the NIR fluorescence emission of cypate.

EXPERIMENTAL SECTION

General

All reagents and solvents were purchased from commercial sources. Solvents and chemicals were reagent grade and used without further purification. Cypate was prepared as we reported previously (45). Analytical (Vydac C-18 column; 250×4.6 mm) and semi-preparative (Vydac C-18 column; 25×2.2 cm) HPLC were performed at a flow rate of 1.0 mL/min and 9.5 mL/min, respectively. HPLC solvents consisted of solvent A (water containing 0.05%

trifluoroacetic acid, TFA) and solvent B (acetonitrile (ACN) containing 0.05% TFA). Linear gradient elution protocol for analytical HPLC started from 90% A to 30% A in B for 20 min. The gradient for semi-preparative HPLC ranged from 90% A to 30% A over 15 min and held at 30% for 30 min. The elution profile was monitored by UV/Vis at 214 nm and 254 nm. Mass spectra (ES-MS) were obtained using Shimadzu mass spectrometer (LCMS-2010A) in the positive electrospray mode.

Solid phase peptide synthesis

All the peptides were assembled manually on resin using conventional Fmoc chemistry (46). The coupling reactions were carried out by adding a pre-activated solution of N-α-Fmoc-protected amino acid (3 equiv), 1-hydroxybenzotriazole (HOBt, 3 equiv), 2-(1H-benzotriazole-1-yl)-1,1,3,3-tetramethyluronium hexafluorophosphate (HBTU, 3 equiv), and N,N-diisopropylethylamine (DIEA, 6 equiv) in anhydrous *N*,*N*-dimethylformamide (DMF, 3 mL/g resin) to the resin (1 equiv) and mixing for 2 h. The progress of the coupling was monitored by the Kaiser test. The Fmoc protecting group was removed by treating the product with a solution of 20% piperidine in DMF for 10 min (2X). The resin was washed with methanol (1 min, 3 mL, 2X) and DMF (1 min, 3 mL,6×) and used in subsequent reactions.

Cyclo[Asp(OBut)-phe-Lys-Arg(Pbf)-Gly]

The resin-bound protected peptide (H-Asp(OBut)-phe-Lys-Arg(Pbf)-Gly-resin) was assembled manually from H-Gly-2-chlorotrityl resin (1.0 g, 0.54 mmol/g) as described above. The side-chain protected peptide was cleaved by mixing the resin with 1% TFA in dichloromethane (DCM) for 5 min. The filtrate was added to a solution of pyridine (5 mL)/methanol (10 mL) and the resin was washed with methanol and dichloromethane. The cleavage procedure was repeated 5 times. The combined filtrate afforded the desired protected RGD pentapeptide (H-phe-Lys(Dde)-Arg(Pbf)-Gly-Asp(OBut)-OH; 561 mg, 95% yield, ES-MS: $[MH]^+/[MH]^{2+}$ 1094.5/547.8).

The linear peptide obtained was added dropwise into a solution of benzotriazole-1-yl-oxy-tris-pyrrolidino-phosphonium hexafluorophosphate (PyBOP, 520 mg, 1.0 mmol), HOBT (135 mg, 1.0 mmol), and DIEA (207 mg, 1.6 mmol) in DMF (80 mL)/DCM (720 mL). The mixture was stirred overnight, concentrated, and washed with water to give the crude product cyclo[Asp(OBut)-phe-Lys(Dde)-Arg(Pbf)-Gly] (ES-MS: $[MH]^+$ 1076.3). The solid was dissolved in ACN (47.5 mL)/water (2.5 mL), followed by adding hydrazine (2.5 mL). The mixture was stirred for 15 min, concentrated, washed with water, and dried. The product, cyclo[Asp(OBut)-phe-Lys-Arg(Pbf)-Gly], was further purified by column chromatography (silica gel, methanol/dichloromethane) to afford the desired compound (295 mg, 60% yield, ES-MS: $[MH]^+$ 912.3).

Cypate-cyclo[phe-Lys(~)-Arg(Pbf)-Gly-Asp(OBut)] and cypate-cyclo[phe-Lys(~)-Arg-Gly-Asp] (2)

The protected cyclic peptide obtained above (50 mg, 0.05 mmol) was swirled with a mixture of cypate (141 mg, 0.2 mmol), HOBT (13 mg, 0.1 mmol), and N-(3-dimethylaminopropyl)-N′-ethylcarbodiimide hydrochloride (EDAC, 29 mg, 0.15 mmol) in DMF (2.0 mL) overnight. The mixture was concentrated to afford the crude product (ES-MS: $[MH_2]^{2+}$ 759.8) and split into two portions, one of which was dissolved in a mixture of TFA: water (95:5) and deblocked for 4 h. The TFA mixture was added to cold methyl *tert*-butyl ether (MTBE, 10 mL). Finally, the solid precipitate was collected by filtration and purified by HPLC to afford the desired product cypate-cyclo[phe-Lys(~)-Arg-Gly-Asp] (9.mg, 13% yield, ES-MS: $[MH]^+/[MH_2]^{2+}$ 1210.3/606.0).

DFO-cypate-cyclo[phe-Lys(~)-Arg(Pbf)-Gly-Asp(OBut)] and DFO-cypate-cyclo[phe-Lys(~)-Arg-Gly-Asp] (1)

A mixture of DFO (106 mg, 0.15 mmol) and DIEA (19.4 mg, 0.15 mmol) in DMSO (3 mL) was sonicated to obtain a clear solution. The solution was added to cypate-cyclo[phe-Lys(~)-Arg(Pbf)-Gly-Asp(OBut)] (80 mg, 0.05 mmol) in DMF (3 mL), followed by addition of EDCI (29 mg, 0.15 mmol) and HOBT (21 mg, 0.15 mmol). The mixture was stirred for 3 h and concentrated under high vacuum. Addition of the residue to water (5 mL) precipitated the product, which was collected and purified by HPLC to obtain DFO-cypate-cyclo[phe-Lys(~)-Arg(Pbf)-Gly-Asp(OBut)] (27 mg, 25% yield, ES-MS: $[MH]^{2+}$ 1031.6). The resultant solid (20 mg) was dissolved in TFA (1 mL) and kept at room temperature for 2 h. The TFA solution was concentrated and purified by semi-preparative HPLC to afford DFO-cypate-cyclo[phe-Lys(~)-Arg-Gly-Asp] (7 mg, 40% yield, ES-MS: $[MH]^{2+}/[MH_2]^{3+}$ 877.2/585.1).

Cypate-DFO (3)

Deferoxamine mesylate salt (131 mg, 0.2 mmol) was dissolved in DMSO (3 mL) in the presence of DIEA (26 mg, 0.2 mmol) by sonication, followed by adding HOBT (27 mg, 0.2 mmol), cypate (141 mg, 0.2 mmol), and N-(3-Dimethylaminopropyl)-N′-3-ethylcarbodiimide hydrochloride (EDCI, 38 mg, 0.2 mmol). The mixture was stirred at room temperature for 2 h and added with stirring to ether. The precipitate was collected by filtration, one third of which was purified by HPLC to afford cypate-DFO (25 mg, 30%, ES-MS: $[MH]^{+}/[MH]^{2+}$ 1167.1/584.4).

Absorption and Emission Spectral Analysis

Absorption and fluorescence spectra were recorded on a DU 640 UV-Visible spectrophotometer and Fluorolog-3 fluorometer, respectively. Stock solutions (1.0 mM) of the dye and its conjugates were prepared by dissolving each sample in 80% aq. DMSO, unless otherwise stated. UV-Vis and fluorescence measurements were carried out by sequentially adding 5.0 μL aliquots of the stock solutions via a micropipette into 3 mL of 20% aq. DMSO solution in a quartz cuvette. The fluorescence quantum yields of **1, 2, 3**, cypate, and ICG in PBS pH =7.4 and DMSO were determined according to an established protocol and referenced to ICG in DMSO (Q.Y. =0.13). The absorbance of five serial dilutions of each compound was measured in the concentration range between 0.1–1.0 μM. The quantum yield (Φ) was determined according to the following equation (47):

$$\Phi_s = \Phi_r (Grad_s / Grad_r)(\eta_s^2 / \eta_r^2)(q_s / q_r)$$

where the subscripts *s* and *r* refer to sample and reference ICG (obtained by HPLC purification of commercially available ICG from Aldrich), respectively. η represents the refractive index of the solvent, and *q* represents a correction factor accounting for the excitation wavelength used. q_s/q_r was assumed to be 1 under similar excitation conditions.

Metal binding studies

Stock solutions (1 mM) of compounds **1**, **3**, and DFO were first prepared with 50% aq. ACN. We also prepared stock solutions of the following metal salts in distilled water:$Fe(NO_3)_3$, $FeSO_4$, $Al_2(SO_4)_3$, $Ga_2(SO_4)_3$, $InCl_3$, $GdCl_3$, $CuSO_4$, $ZnSO_4$, $Co(NO_3)_2$, $NiCl_2$, $MnCl_2$, $CaCl_2$, $MgCl_2$, and $MgSO_4$. All test solutions (100 μL each) containing 100 μM of a ligand and 200 uM of a metal ion were prepared by mixing compounds **1**, **3**, or DFO (10 μL, 1.0 mM) and a metal ion (20 μL, 1.0 mM) in 70 μL of 50% aq. ACN. After the solutions were stirred for 2 h, 20 μL of the resulting solutions were subjected to ESI-MS analysis. Each solution (30.0 μL) was added to 2970.0 μL of 20% aq. DMSO for UV-Vis and fluorescence emission analysis.

ABIR binding affinity

Receptor binding assays were performed by using human purified ABIR protein from Chemicon International, Inc. (Temecula, CA) using the method reported previously (48). Briefly, assays were carried out in the Millipore Duropore membrane 96-well plates and the Millipore MultiScreen system (Bedfore, MA). ^{125}I echistatin was purchased from Amersham Biosciences (Piscataway, NJ) carried. The specific activity of the radiolabeled peptide was ~2000 Ci/mmol. Radiochemical purity (90%) was determined by reverse phase HPLC. The 96-well membrane plate was blocked with 0.1% polyethylenimine blocking solution overnight at 4 °C. ^{125}I-echistatin (50 nmol/L) was added to the binding buffer (50 mM Tris-HCl, pH 7.4, 100 mM NaCl, 2 mM $CaCl_2$, 1 mM $MgCl_2$, 1 mM $MnCl_2$, 1 % BSA) containing integrin ABIR protein (50 ng per well in 96-well membrane plate) and ligands in a total volume of 200 μL per well. The concentration range of ligand was between 0.01 μM and 100 μM. The mixtures were incubated for 2 h at room temperature, filtered by centrifugation at 1500 g, and washed with 0.20 mL of ice-cold binding buffer (3X). The filters containing radioactivity bound ABIR were removed using a punch apparatus and counted using a Packard Cobra II Auto-gamma counter (Meriden, CT). Nonspecific binding of ^{125}I-echistatin was between 5 to 10% of the total binding. The 50% inhibitory concentrations (IC_{50}) were calculated by nonlinear regression analysis usingGraphPad Prism 4 data fitting software (GraphPad Software, Inc., San Diego, CA). Three independent binding assays were performed in triplicates per sample.

Cell Culture

The human non-small cell carcinoma cell line A549 is widely used to study the role of integrins in normal and pathophysiological processes. These cells were purchased from ATCC and grown in 75 cm tissue culture flasks or on Lab-Tek chambered slides in Ham's F12K medium with 2 mM L-glutamine supplemented with 1.5 g/L sodium bicarbonate, 10% fetal calf serum, 100 units/mL Penicillin and 100 units/mL Streptomycin under humidified atmosphere containing 5% CO_2 at 37 °C.

Internalization and fluorescence microscopy

A549 cells were grown on Lab-Tek slides. The culture medium was replaced and the cells were incubated for different times up to 24 h at 37 °C in the presence of the cypate-labeled DFO probes (1 μM in 0.02% DMSO). After treatment, cells were washed (3X) with PBS containing 1 mM $CaCl_2$ and mounted with Prolong Gold containing DAPI mounting medium and coverslipped (Invitrogen). For fluorescence microscopy, cells were visualized with Olympus FV1000 microscope using a 60X/1.20M, 0.13–0.21 NA water immersion objective. Fluorescence emission was detected from 805 – 830 nm using a 780 nm laser at 100% transmission for excitation. Images of each group of slides were acquired with the same microscope settings during a single imaging session, allowing for qualitative comparison of the relative fluorescence. The relative fluorescence intensity of five regions of interest for each image was determined with Slidebook software from Olympus and the results averaged. The results were normalized to the average relative fluorescence of DFO-cypate treated cells.

For mitochondrial staining, 5 nm Mitotracker Green (Invitrogen) was added during the last 15 min of incubation. For lysosomal staining, cells were stained with anti-LAMP1 antibody as described in the literature (49). Briefly, cells were fixed for 15 min with 4% paraformaldehyde for 15 minutes, after which they were washed three times with PBS containing 1 mM $CaCl_2$. Slides were incubated for 1h at room temperature with 10% rabbit serum to block non-specific binding after which they were incubated overnight at 4 °C with 2 μg/mL anti-LAMP1 goat polyclonal IgG (Santa Cruz). After washing 3× with PBS, slides were incubated for 1h at room temperature with 10 μg/mL Cy3 conjugated rabbit anti-goat IgG (Zymed). After washing 3x with PBS, slides were mounted with Prolong Gold and coverslipped. Cells were visualized with Olympus FV1000 microscope using a 60X/1.20M, 0.13–0.21 NA water immersion

objective. Fluorescence emission was detected from using a 488 nm laser at 5% transmission and 500–600 nm emission (Mitotracker green) or using a 543 nm laser at 15% transmission and 555–655 nm emission (LAMP-1).

RESULTS AND DISCUSSION

Molecular Design

Previously, we reported the synthesis and applications of a di-carboxylic acid-containing carbocyanine fluorophore (cypate) (10,45). The facile synthesis of cypate and its excellent NIR spectral properties have allowed us to label diverse peptides and other bioactive molecules with cypate in solution and on solid support conveniently. Particularly, the two carboxylic acid groups of cypate have facilitated its use as an optical scaffold to construct diverse bioactive NIR fluorescent molecular probes such as monomeric, dimeric, macrocyclic, and multivalent analogs (8,45,50,51). Conjugation of cypate with small peptides that target specific cell surface receptors such as ABIR and somatostatin receptor allows site-specific targeting of diseased tissues for optical imaging (9,10,51). In particular, previous reports have shown that cyclic RGD pentapeptide cyclo(RGDfV) and some of its analogs bind to ABIR with high affinity and selectivity. Further modification of the biological properties of cypate-labeled RGD peptides could be obtained by incorporating another bioactive molecule such as DFO.

The metal binding properties and the related biological activities of DFO have been ascribed to its three hydroxamate groups (26,52). Therefore, the amino group of DFO provides a desirable site for its structural modification. In this work, we used cypate to construct a three-pronged architecture bearing both DFO motif and ABIR-targeting RGD peptide (cyclo [RGDfK(~)] (Figure 1). We anticipated the new NIR fluorescent RGD-bearing DFO compound (**1**) could serve as a multifunctional platform for biomedical applications. For example, RGD peptide motif could be used for targeted delivery of DFO to ABIR positive tumors while cypate serves as the optical antenna to track, visualize, and quantify the fate of **1** in cells and in vivo by NIR fluorescence imaging. In addition, the integration of DFO and RGD peptide into cypate could cooperatively enhance the related biological activities. Finally, the metal binding DFO could modify the structure, function, and regulation of divalent cation-dependent ABIR (28,38). Together, these potential applications of NIR fluorescent DFO compounds motivated the design, synthesis, and evaluation of the compounds described in this report.

Synthesis

As shown in Scheme 1, synthesis of the multifunction compound **1** consists of three major steps: (i) synthesis of the protecting RGD peptide, (ii) cypate conjugation, and (iii) DFO conjugation. The resin-bound protected RGD penta-peptide, H-Asp(OBu^t)-phe-Lys(Dde)-Arg (Pbf)-Gly-O-Resin (**1**), was first assembled on a H-Asp(Bu^t) loaded 2-chlorotrityl resin using conventional Fmoc chemistry. Cleavage of the protected peptide with 1% TFA in DCM afforded the desired protected RGD pentapeptide, H-phe-Lys(Dde)-Arg(Pbf)-Gly-Asp (OBu^t)-OH. This linear peptide was cyclized to form cyclo[phe-Lys(Dde)-Arg(Pbf)-Gly-Asp (OBu^t)] in the presence of PyBOP, HOBT, and DIEA in solution. Removal of the ε-amino lysine protecting Dde group with hydrazine in methanol afforded cyclo[phe-Lys-Arg(Pbf)-Gly-Asp(OBu^t)], which was further purified by flash column chromatography. Similarly, the conjugation of the cyclic peptide (1 equiv) and cypate (3 equiv) was achieved in the presence of EDCI and HOBT in anhydrous DMF. The crude product, cypate-[Arg(Pbf)-Gly-Asp(OBut)-phe-Lys(~)], was coupled with DFO, as reported previously (53). Aqueous TFA was used to deblock the resultant product, DFO-cypate-[Arg(Pbf)-Gly-Asp(OBut)-phe-Lys(~)], which was then purified by HPLC to give the desired compound **1**, DFO-cypate-cyclo[Arg-Gly-Asp-phe-Lys]. The identity and purity of the compound were identified by both HPLC and ES-MS.

A combination of solution and solid phase reactions facilitated the preparation if all compounds used in this study by a similar protocol.

Spectral properties

Stock solutions (1 mM) of the DFO-containing compounds were prepared in DMSO and spectral measurements were carried out by adding 2.0 μL aliquots of the stock solutions via a micropipette into 3 mL of DMSO solution in a quartz cuvette. All the compounds showed similar spectral features, with minor spectral shifts in the absorption and emission maxima (Figure 2). The attachment of cyclo[RGDfK(~)] to cypate increased the molar absorptivity (ε) while the DFO attachment decreased ε (Table 1). Compound **1** containing both DFO and cyclo[RGDfK(~)] showed similar ε with cypate. Overall, conjugation of the highly hydrophilic DFO to cypate improved the water solubility of the dye without adverse effect on its spectral properties.

Metal binding studies

Siderophores such as DFO are good ligands for Fe(III) and the biological activities of DFO are related to its metal binding properties (20,54–56). Previous studies have shown that DFO and the related hydroxamate compounds also possess high binding affinities with Al(III) and Ga(III) (26,53). Therefore, we evaluated the metal binding properties of **1** and the related effects on the corresponding optical properties of DFO-bearing fluorescent compounds. Because of its high sensitivity, we used ES-MS to study the metal coordination with DFO, as described previously (26,57). This method is suitable for screening the relative metal-binding selectivity and affinity of some compounds, especially those in limited supply.

Compounds **1**, **3** and DFO (100 μM in 50% aqueous acetonitrile) were screened for their binding with 13 different metal ions Fe(III), Al(III), Ga(III), In(III), Gd(III), Cu(II), Zn(II), Co (II), Ni(II), Mn(II), Fe(II), Ca(II), and Mg(II) at 200 μM in water. All the three DFO-bearing compounds exhibited high binding affinity and selectivity for Ga(III), Al(III), and Fe(III) compared to the other metal ions. The ES-MS spectra of **1** and the metal chelates shown in Figure 3 are representative of the trend observed for these compounds. Compound **1** showed two typical doubly and triply charged peaks at 876.7 and 584.9 in its ES-MSI spectrum. Upon metal binding, these peaks were replaced by the corresponding doubly charged (903.5, 889.0, 910.1) and triply charged (602.2, 592.8, and 607.5 peak) peaks of the resulting Ga(III), Al(III), and Fe(III) complexes, respectively. These peaks correlated with the theoretical masses based on $[(L\text{-}3H)MH_n]^{n+}$, where L and M represent the molecular weight of a ligand and a metal, respectively. The high abundance of the desired metal chelate peaks with negligible residue from the starting DFO ligand strongly suggest the complete formation of 1:1 metal complexes in aq. ACN.

We further calculated the relative metal-binding affinity (%) of each ligand as a percentage of the relative abundance of the metal binding ligand peaks with the total ligand-related peaks in a positive ES-MS spectrum according to the following equation, as reported previously (26, 58):

$$[LFe^2+LFe^3]/[L^2+L^3+LFe^2+LFe^3+L+LFeNa^2+LFeNa^3] \times 100(\%)$$

where L^2 and LFe^2 are the doubly charged peaks abundance of a ligand and its complex while L^3 and LFe^3 are the triply charged peak abundance of a ligand and its complex. The related peaks associated with the addition of sodium ions were also calculated. As showed in Figure 4, the ES-MS analysis clearly demonstrated the relative metal binding selectivity and affinity with Fe(III), Fe(II), Ga(III), Al(III), and In(III). Despite their structural differences, the metal

binding selectivity of **1**,**3**, and DFO was similar, indicating that the chelating property of DFO was maintained, independent of the molecular design.

In contrast to the ES-MS spectra of Ga(III) and Al(III), the addition of Fe(III) and Cu(II) resulted incomplicated ES-MS spectra with multiple peaks around the doubly and triply charged peaks. This observation suggests that Cu(II) had weak binding with **1,** but might greatly impact the ionization of 1 and stability of the resulting ions in gas phase. In addition, the low abundance of the related 1:1 ligand:metal complex indicates that Cu(II) binding might occur between two or more ligand **1** with two or more Cu(II).

The relatively high binding affinity of DFO bearing compounds with Fe(III), Al(III), and Ga (III) makes it possible to further functionalize **1** via metal binding. Therefore, we prepared and isolated the Ga(III) complex of **1** to demonstrate the feasibility of obtaining fluorescent DFO chelates. By mixing **1** with excess Ga(III) in aq. ACN, the Ga(III) complex was obtained after HPLC purification and further characterized by ES-MS. The metal complex has a longer retention time than **1** because coordination of Ga(III) by the three DFO hydroxamates reduces the hydrophilicity of **1** (Figure 5). The successful preparation and characterization of the Ga (III) complex provides an exciting dimension to explore additional applications of this compound in biomedicine.

Spectrally, there was no significant change in the green color of **1** upon the additions of the metals, with the exception of Fe(III), Fe(II), and Cu(II), where a change was observed (Figure 6). Clearly, the addition of Cu(II) and Fe(III) markedly decreased the UV-Vis absorption and quenched the fluorescence emission of **1** as shown in Figure 6. Based on the ES-MS analysis discussed above, it is likely that spectral changes by these metals occurred by different mechanisms. While Cu (II) appears toquench fluorescence by interacting directly with the polymethine chain of cypate, the stable Fe complex may quench fluorescence by photoinduced electron transfer mechanism. In contrast to Fe(III) and Cu(II), the Ga(III) binding did not alter significantly the UV-Vis absorbance of **1**. Interestingly, Ga(III) seemed to enhance light emission to some extent. This finding is in agreement with a previous study with **3** where a similar enhancement was observed(53). Considering that a DFO chelate of radioactive Ga(III) has been used previously for nuclear imaging, the Ga(III)-mediated fluorescence enhancement favors the use of the Ga(III) complex of compounds **1** and **3** to develop a dual optical-nuclear imaging agent. In addition, the contrasting effects of Fe(III) and Ga(III) on the optical properties of cypate provides an efficient approach to perturb the spectral properties of NIR fluorescent carbocyanine probes via metal binding.

Receptor binding assays

Among the diverse RGD peptides that have been developed for targeting ABIR, the lactam-based cyclic penta-peptide cyclo(RGDfV) and its analogs are well-known for their high binding affinity and selectivity with ABIR. In this study, commercially available ABIR-avid peptide cyclo(RGDfV) was used as a reference compound to study the effect of DFO on ABIR binding affinity of **1** and **2**. The IC_{50} values of these compounds were determined by competitive inhibition of Echistatin binding to purified ABIR, as described previously (48,59). Echistatin is a polypeptide that binds irreversibly with high affinity and specificity to the ABIR and the radiolabeled analog ^{125}I-echistatin was used as a tracer in the binding assay. Compounds **1**, **2**, and cyclo(RGDfV) were found to have IC_{50} values of 1.8×10^{-7} M, 7.7×10^{-8} M, and 4.1×10^{-7} M, respectively. Under similar conditions, the presence of DFO motif in **1** decreased the ABIR affinity of **2** by a factor of about 2 but the resulting affinity was comparable to the reference cyclic RGD compound. These findings indicate the RGD peptide can modulate the biological activities of DFO through receptor-mediated delivery of this otherwise nonspecific drug to target tissue and cells.

Cell internalization

Uptake and distribution of drugs and contrast agents in cells provide a key index for understanding the functions and predicting the in vivo behavior of fluorescentcompounds. Therefore, labeling DFO with fluorescent dye allows the use of the resultant molecule as molecular probe for imaging DFO distribution in cells. Considering that the ABIR binding assay revealed retention of RGD peptide binding affinity by **1**, we assessed the internalization and subcellular distribution of **1**, **2**, and **3** in an ABIR-positive cell line, A549. The incubation of A549 cells with **3** (1μM) in medium containing 0.02% DMSO showed minimal uptake of the compound, with normalized fluorescence similar to background signal (Figure 7). Expectedly, hydrophilic molecules such as DFO have difficulty crossing the plasma membranes of cells without an active transport mechanism. In contrast, both **1** and **2** internalized rapidly within 1 h post incubation and remained in the intracellular space up to 10 h. The enhanced internalizations of **1** and **2** could be ascribed to the interaction of the RGD peptide with ABIR in the cell membranes. Thus, the RGD peptide provided an endocytotic pathway for DFO. At 1 h post-incubation, the internalization of **1** and **2** in A549 cells was similar to each other but the retention of **1** in the cells was lower at longer incubation times than **2** (Figure 7D). The differences in the internalization rate appear to correlate with their ABIR binding affinity, with **2** having higher affinity than **1**. Once internalized, however, the ratesof subsequent efflux of the two compounds from the cell were similar, with the intracellular fluorescence intensity for both compounds approaching background at 24 h post incubation. The fluctuations in fluorescence shown in Figure 7D could be attributed to changes in receptor density as a function of time.

Based on the dissimilarity in structural features, ABIR binding affinity, and internalization rates, we expected differences in the intracellular distribution of compounds **1**, **2**, and **3**. Interestingly, once inside the cell, all 3 compounds appeared to localize in the mitochondria, the lysosomes and the cytosol (Figures 8 and 9). The absence of identifiable uptake in the cell nuclei favors using the fluorescent DFO compounds as imaging agents because of the need to minimize nuclear translocation of imaging agents, thereby preventing potential mutagenic effect on the cells.

CONCLUSION

We have developed a novel multifunctional molecular probe consisting of a metal chelating DFO, a NIR fluorescent cypate, and an ABIR-avid cyclic RGD peptide. Each component synergistically contributes to the overall properties of the new compound **1**. Cypate provides detectable signal for imaging purposes, RGD peptide effectively delivers both cypate and DFO into cells, and DFO efficiently modulates the optical properties of cypate. The impressive ABIR-mediated internalization of **1** in cells without permeating the cell nucleus is advantageous for imaging applications, where nuclear uptake can be detrimental to the cells and living organisms. This work represents our initial effort toward the discovery and development of novel ABIR-targeting DFO compounds for optical imaging. Specifically, **1** provides a multifunctional molecular platform for optimizing the structure, improving the biological activities, exploring new applications, and understanding the mechanisms of action. The synthetic approach we used is amenable to combinatorial chemistry and parallel synthesis of diverse NIR fluorescent DFO analogs.

Acknowledgements

This study was supported in part by the NIH (R01 CA109754, R33 CA100972, and R21 CA123537).

LITERATURE CITED

1. Kelloff GJ, Krohn KA, Larson SM, Weissleder R, Mankoff DA, Hoffman JM, Link JM, Guyton KZ, Eckelman WC, Scher HI, O'Shaughnessy J, Cheson BD, Sigman CC, Tatum JL, Mills GQ, Sullivan DC, Woodcock J. The progress and promise of molecular imaging probes in oncologic drug development. Clin Cancer Res 2005;11:7967–85. [PubMed: 16299226]
2. El-Deiry WS, Sigman CC, Kelloff GJ. Imaging and oncologic drug development. J Clin Oncol 2006;24:3261–73. [PubMed: 16829650]
3. Apisarnthanarax S, Chao KS. Current imaging paradigms in radiation oncology. Radiat Res 2005;163:1–25. [PubMed: 15606303]
4. Toms SA, Konrad PE, Lin WC, Weil RJ. Neuro-oncological applications of optical spectroscopy. Technol Cancer Res Treat 2006;5:231–8. [PubMed: 16700619]
5. Harada H, Kizaka-Kondoh S, Hiraoka M. Optical imaging of tumor hypoxia and evaluation of efficacy of a hypoxia-targeting drug in living animals. Mol Imaging 2005;4:182–93. [PubMed: 16194450]
6. Schellenberger EA, Bogdanov A Jr, Petrovsky A, Ntziachristos V, Weissleder R, Josephson L. Optical imaging of apoptosis as a biomarker of tumor response to chemotherapy. Neoplasia 2003;5:187–92. [PubMed: 12869301]
7. Perlitz C, Licha K, Scholle FD, Ebert B, Bahner M, Hauff P, Moesta KT, Schirner M. Comparison of two tricarbocyanine-based dyes for fluorescence optical imaging. J Fluoresc 2005;15:443–54. [PubMed: 15986163]
8. Achilefu S, Jimenez HN, Dorshow RB, Bugaj JE, Webb EG, Wilhelm RR, Rajagopalan R, Johler J, Erion JL. Synthesis, in vitro receptor binding, and in vivo evaluation of fluorescein and carbocyanine peptide-based optical contrast agents. J Med Chem 2002;45:2003–15. [PubMed: 11985468]
9. Achilefu S. Lighting up tumors with receptor-specific optical molecular probes. Technol Cancer Res Treat 2004;3:393–409. [PubMed: 15270591]
10. Achilefu S, Dorshow RB, Bugaj JE, Rajagopalan R. Novel receptor-targeted fluorescent contrast agents for in vivo tumor imaging. Invest Radiol 2000;35:479–85. [PubMed: 10946975]
11. Chen X, Conti PS, Moats RA. In vivo near-infrared fluorescence imaging of integrin alphavbeta3 in brain tumor xenografts. Cancer Res 2004;64:8009–14. [PubMed: 15520209]
12. Licha K, Riefke B, Ebert B, Grotzinger C. Cyanine dyes as contrast agents in biomedical optical imaging. Acad Radiol 2002;9(Suppl 2):S320–2. [PubMed: 12188261]
13. Licha K, Hessenius C, Becker A, Henklein P, Bauer M, Wisniewski S, Wiedenmann B, Semmler W. Synthesis, characterization, and biological properties of cyanine-labeled somatostatin analogues as receptor-targeted fluorescent probes. Bioconjug Chem 2001;12:44–50. [PubMed: 11170364]
14. Richardson D, Ponka P, Baker E. The effect of the iron(III) chelator, desferrioxamine, on iron and transferrin uptake by the human malignant melanoma cell. Cancer Res 1994;54:685–9. [PubMed: 8306330]
15. Singer ST, Vichinsky EP. Deferoxamine treatment during pregnancy: is it harmful? Am J Hematol 1999;60:24–6. [PubMed: 9883802]
16. Hershko CM, Link GM, Konijn AM, Cabantchik ZI. Iron chelation therapy. Curr Hematol Rep 2005;4:110–6. [PubMed: 15720959]
17. Hershko C, Link G, Konijn AM, Cabantchik ZI. Objectives and mechanism of iron chelation therapy. Ann N Y Acad Sci 2005;1054:124–35. [PubMed: 16339658]
18. Dayani PN, Bishop MC, Black K, Zeltzer PM. Desferoxamine (DFO)--mediated iron chelation: rationale for a novel approach to therapy for brain cancer. J Neurooncol 2004;67:367–77. [PubMed: 15164994]
19. Gao J, Richardson DR. The potential of iron chelators of the pyridoxal isonicotinoyl hydrazone class as effective antiproliferative agents, IV: The mechanisms involved in inhibiting cell-cycle progression. Blood 2001;98:842–50. [PubMed: 11468187]
20. Kicic A, Chua AC, Baker E. Effect of iron chelators on proliferation and iron uptake in hepatoma cells. Cancer 2001;92:3093–110. [PubMed: 11753989]
21. Tam TF, Leung-Toung R, Li W, Wang Y, Karimian K, Spino M. Iron chelator research: past, present, and future. Curr Med Chem 2003;10:983–95. [PubMed: 12678671]

22. Cook J. Radiation sensitization of mammalian cells by metal chelators. Radiat Res 2001;155:304–10. [PubMed: 11175665]
23. Smith-Jones PM, Stolz B, Bruns C, Albert R, Reist HW, Fridrich R, Macke HR. Gallium-67/gallium-68-[DFO]-octreotide--a potential radiopharmaceutical for PET imaging of somatostatin receptor-positive tumors: synthesis and radiolabeling in vitro and preliminary in vivo studies. J Nucl Med 1994;35:317–25. [PubMed: 8295005]
24. Chaston TB, Richardson DR. Iron chelators for the treatment of iron overload disease: relationship between structure, redox activity, and toxicity. Am J Hematol 2003;73:200–10. [PubMed: 12827659]
25. Lovejoy DB, Richardson DR. Iron chelators as anti-neoplastic agents: current developments and promise of the PIH class of chelators. Curr Med Chem 2003;10:1035–49. [PubMed: 12678675]
26. Ye Y, Liu M, Kao JL, Marshall GR. Novel trihydroxamate-containing peptides: design, synthesis, and metal coordination. Biopolymers 2006;84:472–89. [PubMed: 16705688]
27. Ouchetto H, Dias M, Mornet R, Lesuisse E, Camadro JM. A new route to trihydroxamate-containing artificial siderophores and synthesis of a new fluorescent probe. Bioorg Med Chem 2005;13:1799–803. [PubMed: 15698797]
28. Xiong JP, Stehle T, Diefenbach B, Zhang R, Dunker R, Scott DL, Joachimiak A, Goodman SL, Arnaout MA. Crystal structure of the extracellular segment of integrin alpha Vbeta3. Science 2001;294:339–45. [PubMed: 11546839]
29. Liu W, Reinmuth N, Stoeltzing O, Parikh AA, Fan F, Ahmad SA, Jung YD, Ellis LM. Antiangiogenic therapy targeting factors that enhance endothelial cell survival. Semin Oncol 2002;29:96–103. [PubMed: 12138403]
30. Kumar CC. Signaling by integrin receptors. Oncogene 1998;17:1365–73. [PubMed: 9779984]
31. Choe YS, Lee KH. Targeted in vivo imaging of angiogenesis: present status and perspectives. Curr Pharm Des 2007;13:17–31. [PubMed: 17266586]
32. Vellon L, Menendez JA, Lupu R. AlphaVbeta3 integrin regulates heregulin (HRG)-induced cell proliferation and survival in breast cancer. Oncogene 2005;24:3759–73. [PubMed: 15782133]
33. Trikha M, Zhou Z, Timar J, Raso E, Kennel M, Emmell E, Nakada MT. Multiple roles for platelet GPIIb/IIIa and alphavbeta3 integrins in tumor growth, angiogenesis, and metastasis. Cancer Res 2002;62:2824–33. [PubMed: 12019160]
34. Lamfers ML, Grill J, Dirven CM, Van Beusechem VW, Geoerger B, Van Den Berg J, Alemany R, Fueyo J, Curiel DT, Vassal G, Pinedo HM, Vandertop WP, Gerritsen WR. Potential of the conditionally replicative adenovirus Ad5-Delta24RGD in the treatment of malignant gliomas and its enhanced effect with radiotherapy. Cancer Res 2002;62:5736–42. [PubMed: 12384532]
35. Chen X, Plasencia C, Hou Y, Neamati N. Synthesis and biological evaluation of dimeric RGD peptide-paclitaxel conjugate as a model for integrin-targeted drug delivery. J Med Chem 2005;48:1098–106. [PubMed: 15715477]
36. Shen SI, Kotamraj PR, Bhattacharya S, Li X, Jasti BR. Synthesis and characterization of RGD-fatty acid amphiphilic micelles as targeted delivery carriers for anticancer agents. J Drug Target 2007;15:51–8. [PubMed: 17365273]
37. Arap W, Pasqualini R, Ruoslahti E. Cancer treatment by targeted drug delivery to tumor vasculature in a mouse model. Science 1998;279:377–80. [PubMed: 9430587]
38. Xiong JP, Stehle T, Zhang R, Joachimiak A, Frech M, Goodman SL, Arnaout MA. Crystal structure of the extracellular segment of integrin alpha Vbeta3 in complex with an Arg-Gly-Asp ligand. Science 2002;296:151–5. [PubMed: 11884718]
39. Lin HY, Lansing L, Merillon JM, Davis FB, Tang HY, Shih A, Vitrac X, Krisa S, Keating T, Cao HJ, Bergh J, Quackenbush S, Davis PJ. Integrin alphaVbeta3 contains a receptor site for resveratrol. Faseb J 2006;20:1742–4. [PubMed: 16790523]
40. Chen X, Sievers E, Hou Y, Park R, Tohme M, Bart R, Bremner R, Bading JR, Conti PS. Integrin alpha v beta 3-targeted imaging of lung cancer. Neoplasia 2005;7:271–9. [PubMed: 15799827]
41. Chen X, Hou Y, Tohme M, Park R, Khankaldyyan V, Gonzales-Gomez I, Bading JR, Laug WE, Conti PS. Pegylated Arg-Gly-Asp peptide: 64Cu labeling and PET imaging of brain tumor alphavbeta3-integrin expression. J Nucl Med 2004;45:1776–83. [PubMed: 15471848]

42. Cheng Z, Wu Y, Xiong Z, Gambhir SS, Chen X. Near-infrared fluorescent RGD peptides for optical imaging of integrin alphavbeta3 expression in living mice. Bioconjug Chem 2005;16:1433–41. [PubMed: 16287239]
43. Li ZB, Cai W, Cao Q, Chen K, Wu Z, He L, Chen X. 64Cu-Labeled Tetrameric and Octameric RGD Peptides for Small-Animal PET of Tumor {alpha}v{beta}3 Integrin Expression. J Nucl Med 2007;48:1162–71. [PubMed: 17574975]
44. Wu Z, Li ZB, Cai W, He L, Chin FT, Li F, Chen X. (18)F-labeled mini-PEG spacered RGD dimer ((18)F-FPRGD2): synthesis and microPET imaging of alpha (v)beta (3) integrin expression. Eur J Nucl Med Mol Imaging. 2007
45. Ye Y, Bloch S, Kao J, Achilefu S. Multivalent carbocyanine molecular probes: synthesis and applications. Bioconjug Chem 2005;16:51–61. [PubMed: 15656575]
46. White WCWCCPD. Fmoc Solid Phase Peptide Synthesis: A Practical Approach. Feb;2000
47. Li C, Greenwood TR, Bhujwalla ZM, Glunde K. Synthesis and characterization of glucosamine-bound near-infrared probes for optical imaging. Org Lett 2006;8:3623–6. [PubMed: 16898776]
48. Ye Y, Bloch S, Xu B, Achilefu S. Design, synthesis, and evaluation of near infrared fluorescent multimeric RGD peptides for targeting tumors. J Med Chem 2006;49:2268–75. [PubMed: 16570923]
49. Wasylnka JA, Moore MM. Aspergillus fumigatus conidia survive and germinate in acidic organelles of A549 epithelial cells. Journal of Cell Science 2003;116:1579–1587. [PubMed: 12640041]
50. Ye Y, Li WP, Anderson CJ, Kao J, Nikiforovich GV, Achilefu S. Synthesis and characterization of a macrocyclic near-infrared optical scaffold. J Am Chem Soc 2003;125:7766–7. [PubMed: 12822971]
51. Achilefu S, Bloch S, Markiewicz MA, Zhong T, Ye Y, Dorshow RB, Chance B, Liang K. Synergistic effects of light-emitting probes and peptides for targeting and monitoring integrin expression. Proc Natl Acad Sci U S A 2005;102:7976–81. [PubMed: 15911748]
52. Bergeron RJ, Wiegand J, McManis JS, Perumal PT. Synthesis and biological evaluation of hydroxamate-based iron chelators. J Med Chem 1991;34:3182–7. [PubMed: 1956036]
53. Ye, YXB.; Bloch, S.; Achilefu, S. Synthesis, Metal Coordination, and Cellular Internalization of a Siderophore-bearing NIR Fluorescent Carbocyanine Probe. In: Achilefu, Samuel; Bornhop, Darryl J.; Raghavachari, Ramesh, editors. Proceedings of SPIE-The International Society for Optical Engineering (2006), Vol. 6097 60970G-(1–5) (Optical Molecular Probes for Biomedical Applications II). 2006.
54. Jeremy JY, Kontoghiorghes GJ, Hoffbrand AV, Dandona P. The iron chelators desferrioxamine and 1-alkyl-2-methyl-3-hydroxypyrid-4-ones inhibit vascular prostacyclin synthesis in vitro. Biochem J 1988;254:239–44. [PubMed: 3140797]
55. Glickstein H, Breuer W, Loyevsky M, Konijn AM, Shanzer A, Cabantchik ZI. Differential cytotoxicity of iron chelators on malaria-infected cells versus mammalian cells. Blood 1996;87:4871–8. [PubMed: 8639861]
56. Kontoghiorghes GJ. Iron mobilization from transferrin and non-transferrin-bound-iron by deferiprone. Implications in the treatment of thalassemia, anemia of chronic disease, cancer and other conditions. Hemoglobin 2006;30:183–200. [PubMed: 16798643]
57. Tubaro M, Marotta E, Tisato F, Bolzati C, Porchia M, Refosco F, Tomasin P, Cavazza-Ceccato M, Traldi P. Electrospray mass spectrometry of a series of mixed nitrido 99gTc- heterocomplexes conjugated with bioactive molecules. Eur J Mass Spectrom (Chichester, Eng) 2004;10:605–11.
58. Ye Y, Liu M, Kao JL, Marshall GR. Peptide-bond modification for metal coordination: peptides containing two hydroxamate groups. Biopolymers 2003;71:489–515. [PubMed: 14517900]
59. Kumar CC, Nie H, Rogers CP, Malkowski M, Maxwell E, Catino JJ, Armstrong L. Biochemical characterization of the binding of echistatin to integrin alphavbeta3 receptor. J Pharmacol Exp Ther 1997;283:843–53. [PubMed: 9353406]

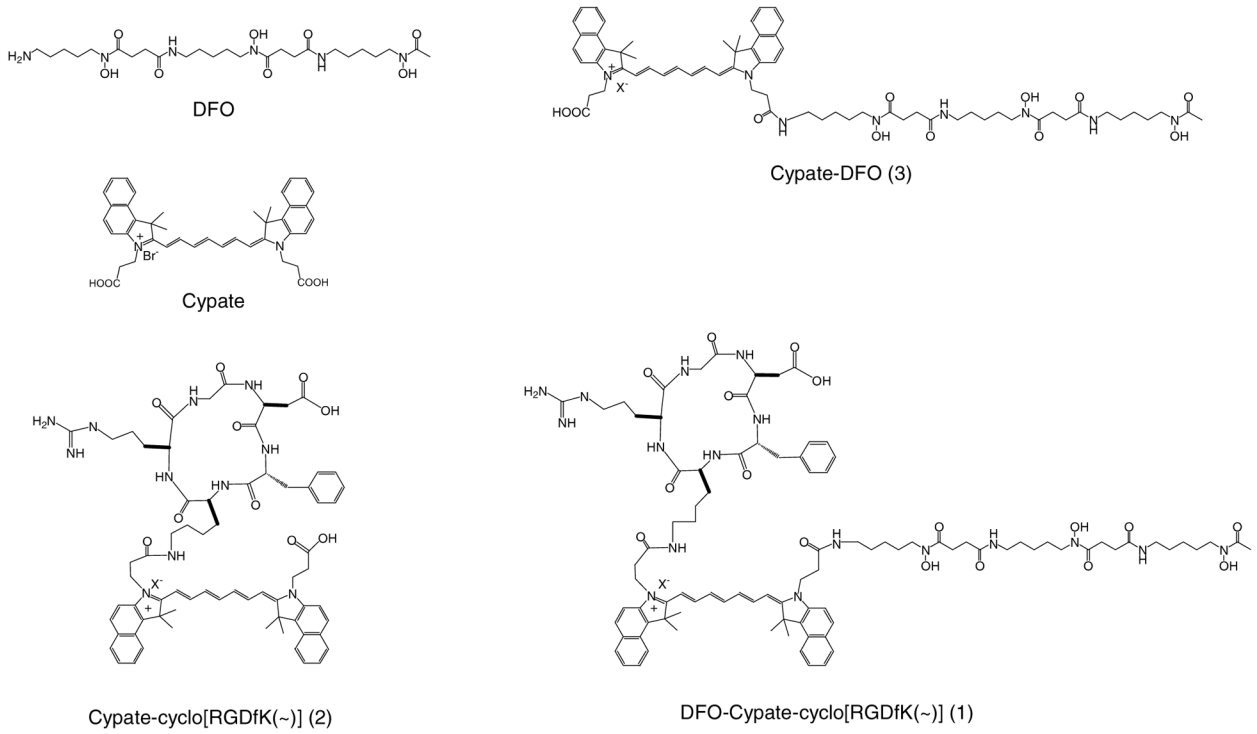

Figure 1.
Structures of DFO-cypate-[RGDfK(~)] (1) and the related compounds.

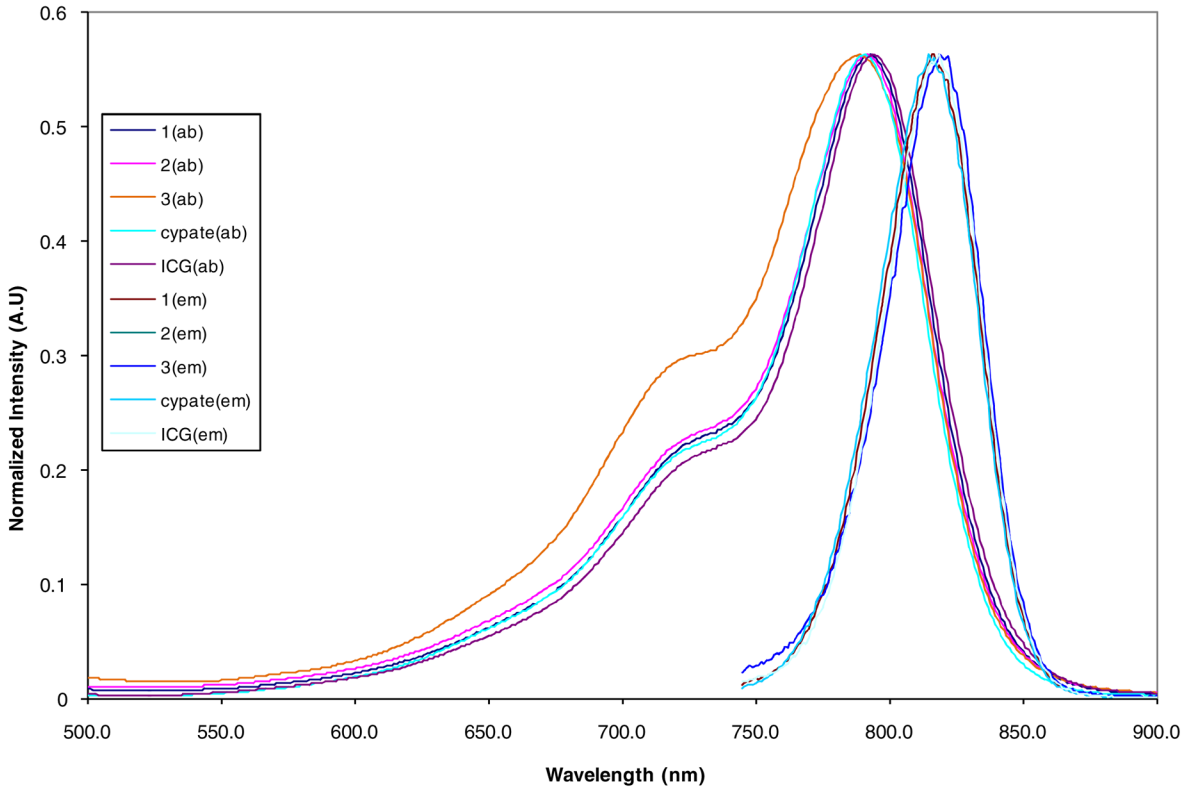

Figure 2.
Normalized UV-Vis and emission spectra of DFO-cypate-[RGDfK(~)] (1), cypate-[RGDfK (~)] (2), and cypate-DFO (3) in DMSO.

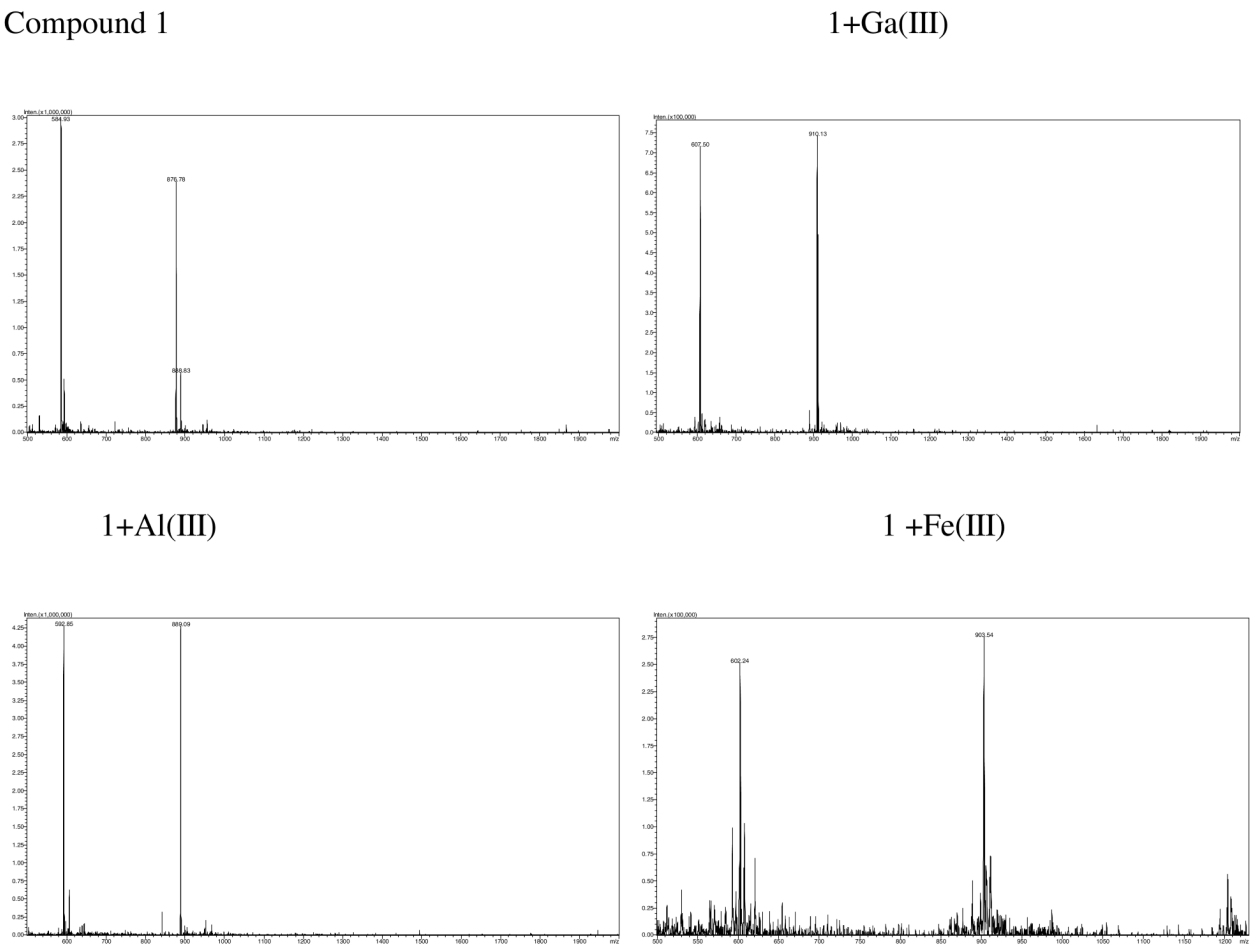

Figure 3.
ES-M spectra of 1 and its Ga(III), Al(III), and Fe(III) complexes (100uM) in 50% aq. ACN.

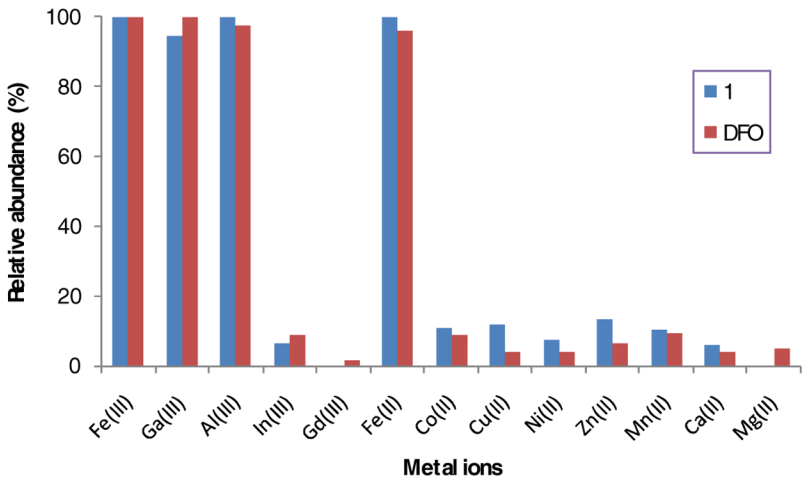

Figure 4.
The relative binding affinities of 1and DFO with different metal ions at a molar ratio of 1:2 as determined by ES-MS.

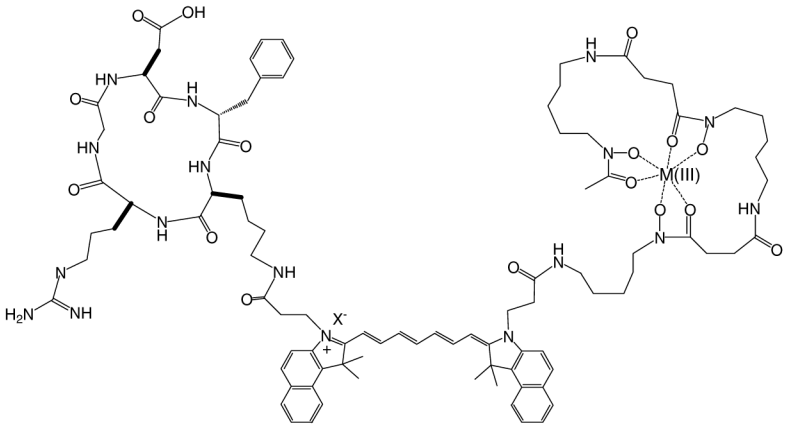

Figure 5.
Proposed metal complex structure of **1**

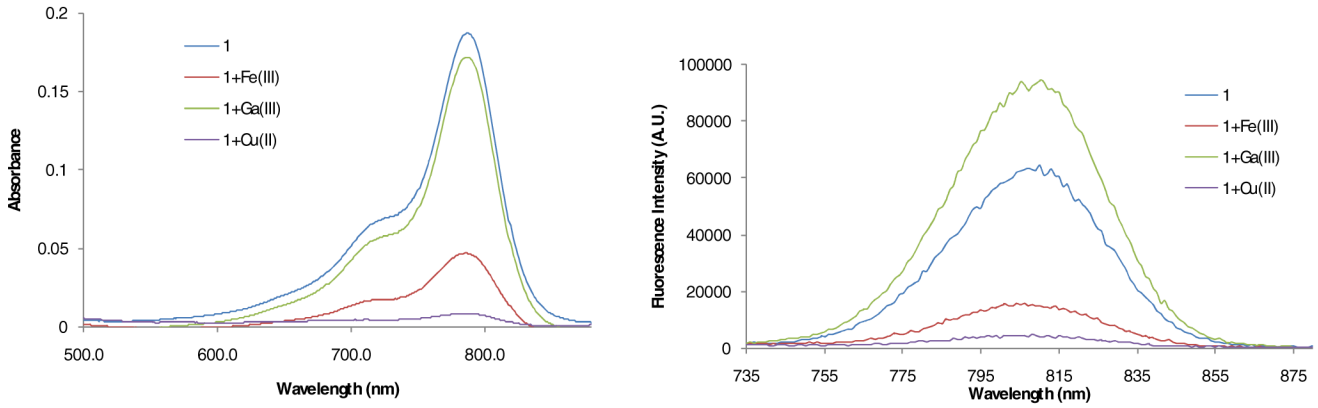

Figure 6.
Effects of Ga(III), Fe(III), and Cu(II) ions on UV-Vis (a, b, and c) and emission (d, e, and f) spectra of **1** in 20% aq. DMSO.

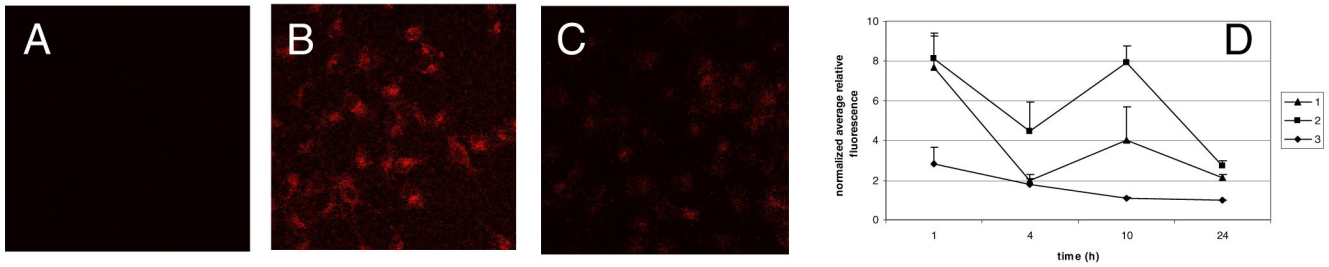

Figure 7.
Internalization in A549 cells treated 10 h with 1 μM of compounds **3** (A), 2 (B) or 1 (C); quantitation of the internalization of each compound as a function of time (D).

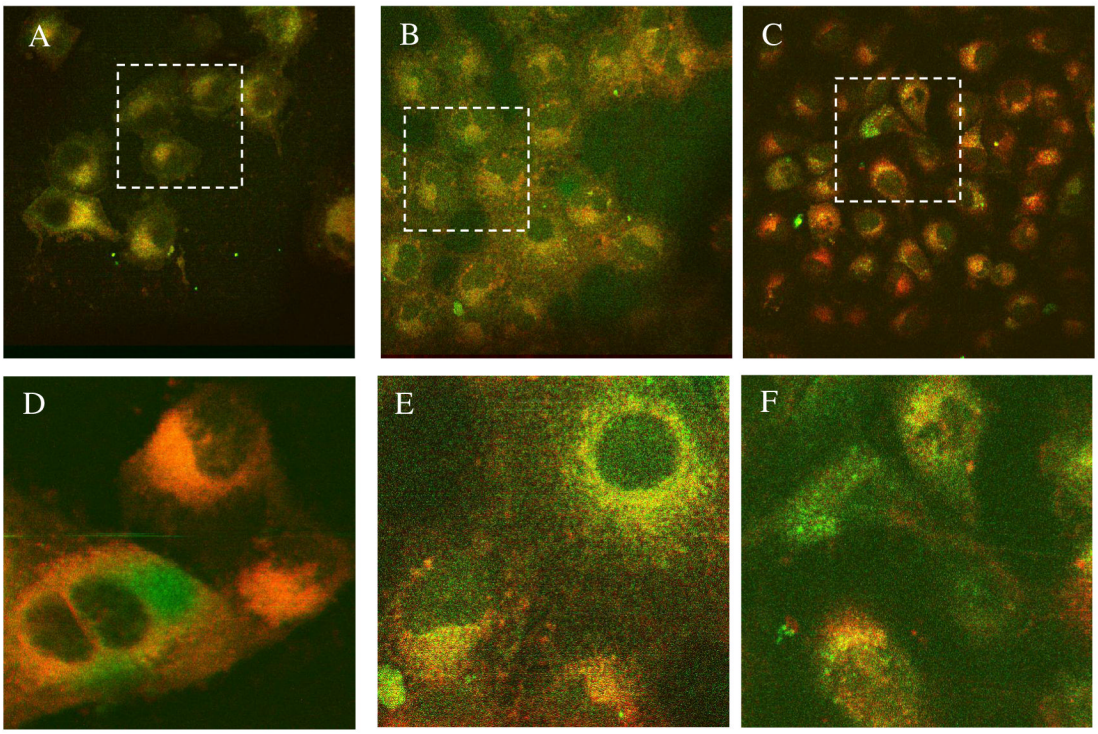

Figure 8.
Subcellular distribution of cells treated 10 h with 1 μM **3** (A), **2** (B) or **1** (C) in medium containing 0.02% DMSO co-stained with Mitotracker green; D, E, F are the inserts at 3x magnification corresponding to A, B, and C, respectively.

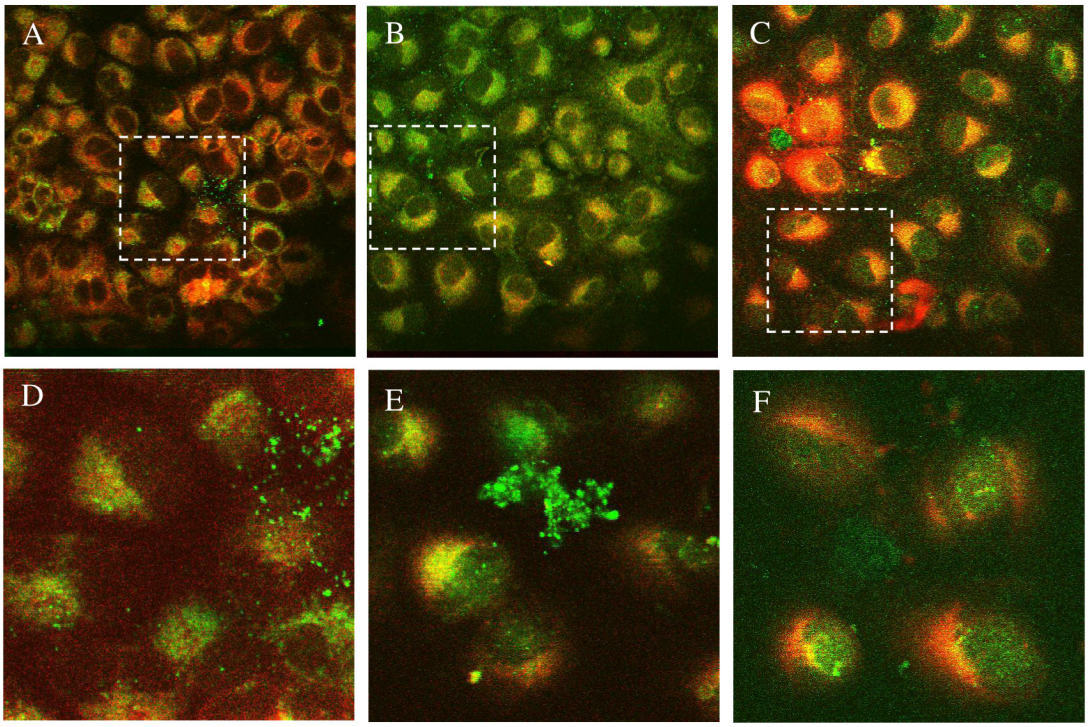

Figure 9.
Subcellular distribution of cells treated 10 h with **3** (A), **2** (B) or **1** (C) co-stained with anti-LAMP1 antibody; D, E, F are the inserts at 3x magnification corresponding to A, B, and C, respectively.

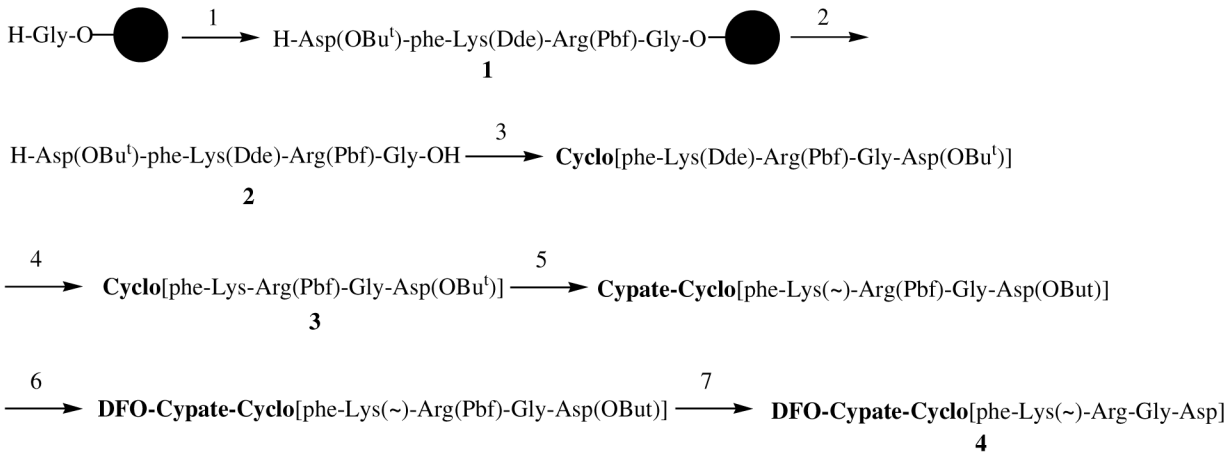

Reagents and conditions: 1. Fmoc chemistry; 2. a) TFA/DCM(1:99); b) Pyridine/DCM/Methanol; 3. PyBOP/HOBT/DIEA/DMF/DCM; 4. Hydrazine/methanol(1:99); 5. **Cypate**/HOBT/DIC/DMF; 6. **DFO**/DIEA/HOBT/EDCI/DMSO; and 7. TFA.

Scheme 1.
Synthesis of DFO-cypate-[RGDfK(~)] (1).

Table 1

Optical properties of the compounds in DMSO

Compounds	$\lambda_{max(ab)}$	$\lambda_{max(em)}$	E ($cm^{-1} M^{-1}$)	*Φ (excited at 730nm)*
1	793	816	2.0×10^5	0.10
2	792	817	2.3×10^5	0.10
3	788	815	1.4×10^5	0.17
cypate	791	814	2.1×10^5	0.12
ICG	794	820	1.9×10^5	0.13